

NANOCERIA PREPARED BY ELECTRON BEAM EVAPORATION

¹Naděžda PIZÚROVÁ, ²Antonín HLAVÁČEK, ^{1,3}Zuzana KAVČIAKOVÁ, ^{1,3}Pavla ROUPCOVÁ,
¹Ivo KUBĚNA, ¹Jiří BURŠÍK, ^{4,5}Sergey Yu. SOKOVNIN

¹*Institute of Physics of Materials, Czech Academy of Sciences, Brno, Czech Republic, EU,
pizurova@ipm.cz, kavciakova@ipm.cz, kubena@ipm.cz, bursik@ipm.cz*

²*Department of Bioanalytical Instrumentation, Institute of Analytical Chemistry, Czech Academy of Sciences,
Brno, Czech Republic, EU, hlavacek@iach.cz*

³*CEITEC - Central European Institute of Technology, Brno University of Technology, Brno, Czech Republic;
EU, roupcova@ipm.cz*

⁴*Institute of Electrophysics Ural Branch RAS, Yekaterinburg, Russia*

⁵*Ural Federal University, Yekaterinburg, Russia; sokovnin@iep.uran.ru*

<https://doi.org/10.37904/nanocon.2022.4585>

Abstract

Cerium oxide nanoparticles (nanoceria) are currently one of the most investigated nanomaterials because of their attractive properties used in biomedical applications, catalysis, fuel cells, and many others. These attractive properties are connected with the Ce³⁺ and Ce⁴⁺ valency state ratio. In the nanoparticle form, cerium oxides contain a mixture of Ce³⁺ and Ce⁴⁺ on the nanoparticle surfaces. Switching between these two states requires oxygen vacancies. Therefore, nanoceria's inherent ability to act as an antioxidant in an environmentally-dependent manner and a "redox switch" to confer auto-regenerating capabilities by automatically shifting between Ce⁴⁺ and Ce³⁺ oxidation states is significantly affected by surface morphology. Regarding this demanded behavior, we aimed to characterize synthesized nanoparticle surface quality and its influence on the cerium oxidation states. The received results were used to evaluate the synthesis method's suitability for suggested utilization.

We used nanoparticles prepared by electron beam evaporation. This unique physical method includes nanoparticle creation through the fast cooling process followed by breaking radiation damaging nanoparticle surfaces to create surface off-stoichiometry. We prepared a sample containing clusters of a mixture of ultra-small nanoparticles and approximately 100 nm particles. X-ray diffraction confirmed the CeO₂ phase in both components. To extract the finest component, we used centrifugal size fractionation. We received 200 nm clusters of 2-10 nm nanoparticles. Nanoparticle shapes and facet types were analyzed using transmission electron microscopy methods. We found out most nanoparticles were formed with truncated octahedrons containing {1,1,1} and {1,0,0} facet types and truncated cuboctahedrons containing {1,1,1}, {1,0,0}, and additional {1,1,0} facets. No octahedron (without truncation) containing only {1,1,1} facets was observed. Nanoparticle shapes containing {1,1,0} and {1,0,0} are suitable for redox activity. Some amount of irregular shapes, beneficial for redox activity, was also observed. Spectroscopy methods confirmed Ce³⁺ content.

Keywords: Nanoceria, Ce³⁺ and Ce⁴⁺, electron beam evaporation, facet types, HRTEM

1. INTRODUCTION

Cerium in compounds exists in two valency states, Ce³⁺ (Ce₂O₃) and Ce⁴⁺ (CeO₂). These valency types are associated with different properties usable for catalysis and biomedical applications, especially for radioprotection of healthy tissues during radiation therapy (Ce⁴⁺) or for supporting radio-oncological treatment toxic effect (Ce³⁺). The formation of oxygen vacancies on the CeO₂ surfaces leads to the reduction of the Ce⁴⁺

ions to Ce^{3+} and vice versa. Such oxygen off-stoichiometry correlates with the redox activity of cerium oxide nanoparticles [1-3].

Cerium oxides formed with the CeO_2 fluorite lattice (**Figure 1a**) contain Ce^{4+} . In the nanoparticle form, CeO_2 contain also Ce^{3+} ions on the surfaces. With a nanoparticle size decrease, the number of surface oxygen vacancies and Ce^{3+} increases [4,5]. Therefore, the $\text{Ce}^{3+}/\text{Ce}^{4+}$ ratio depends on the nanoparticle size. Concurrently, nanoparticle shapes determined with surface facet types can also contribute to this surface effect. Pérez-Bailac et al. [6] demonstrated $\{1,1,0\}$ facets are the most beneficial. The stable nanoparticle shapes are formed with the surface facets of the lowest surface energy. The lowest surface energies for the CeO_2 phase were found for $\{1,1,1\}$ and $\{1,0,0\}$ facets depending on the terminal atomic layer. Table 1 containing the calculated surface energy values shows favorable O-terminated facets in both cases [7]. Considering these values, octahedrons are preferred (**Figure 1b**). This shape is formed with only $\{1,1,1\}$ facet types, unsuitable for vacancy creation. The second lowest energy was found for $\{1,0,0\}$. Therefore, the shapes formed with $\{1,1,1\}$ and $\{1,0,0\}$ are assumed to be the second most favorable nanoparticle forms (**Figure 1c**).

The consideration of the stable morphology, especially nanoparticle shapes and their surface crystallography, is required for redox efficiency and its time stability assessment. For this reason, we analyzed a sample prepared using electron beam evaporation and aged for two years. The high-resolution transmission electron microscopy (HRTEM) analyses, X-ray photoelectron spectroscopy (XPS), X-ray diffraction (XRD), and Electron energy-loss spectroscopy (EELS) were employed for morphological, phase, and oxidation state analyses. TEM samples were purified with centrifugal size fractionation to decrease nanoparticle clusters, receive better nanoparticle distribution, and make more facets visible.

Table 1 Surface energies for $\{1,1,1\}$ and $\{1,0,0\}$ according to the terminal atomic layer [7]

facet	Ce	O	facet	Ce	O
$\{1,1,1\}$	$0.823 \text{ eV}\text{\AA}^{-2}$	$0.084 \text{ eV}\text{\AA}^{-2}$	$\{1,0,0\}$	$0.777 \text{ eV}\text{\AA}^{-2}$	$0.455 \text{ eV}\text{\AA}^{-2}$

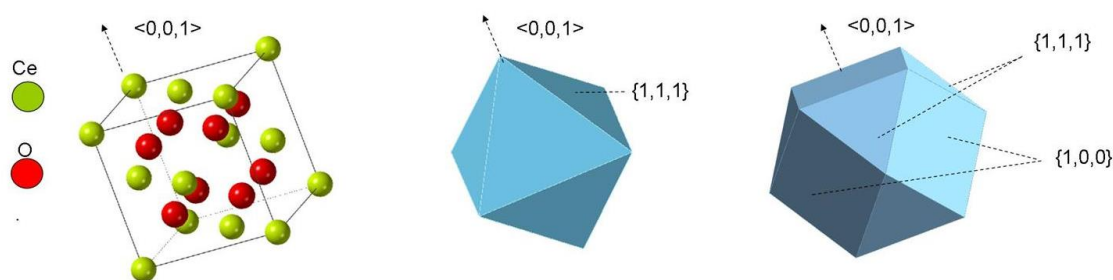


Figure 1 a) CeO_2 lattice, b) octahedron, the most typical CeO_2 nanoparticle morphology containing only $\{1,1,1\}$ facet types, c) cuboctahedron containing $\{1,1,1\}$ and $\{1,0,0\}$ facet types

2. EXPERIMENTAL

2.1. Synthesis - Electron Beam Evaporation

The sample was produced through the evaporation of a solid target (CeO_2 micropowder) by a pulsed electron beam in a H_2 atmosphere using a NANOBEAM 2 device. This method, including the setup for CeO_2 synthesis, was published previously [8].

2.2. Centrifugal Size Fractionation

The sample of nanoparticles (25 mg) was dispersed in a mixture of sodium oleate (1 g), oleylamine (1 g), and octadec-1-ene (5 g). The mixture was supplemented with 5 mL of methanol and slowly heated to $300 \text{ }^\circ\text{C}$ under

a protective N₂ atmosphere (methanol was evaporated at a lower temperature). The temperature of 300 °C was kept for 5 min. After cooling to laboratory temperature (~25 °C), the nanoparticles were precipitated by adding 10 mL of propanol and centrifuged (1500 g, 5 min). The pellet was dispersed in 5 mL of methanol and shortly sonicated in an ultrasonic bath (~20 s). After centrifugation (1500 g, 5 min), the pellet was dispersed in cyclohexane (1 mL) and shortly sonicated (~20 s). The cyclohexane dispersion was centrifuged (1500 g, 5 min), and the supernatant containing the CeO₂ nanoparticles was applied on a TEM grid.

2.3. Chemicals

Centrifugal size fractionation: Methyl alcohol (p.a.), isopropyl alcohol (p.a.), and cyclohexane (p.a.) were from Ing. Petr Švec - PENTA s.r.o. (www.pentachemicals.eu). Sodium oleate (82 %), oleylamine (70 %, technical grade), octadec-1-ene (90 %, technical grade) were from Sigma-Aldrich (www.sigmaldrich.com).

2.4. Characterization Methods

A Titan Themis 60-300 cubed transmission electron microscope was used for morphological analyses. The micrographs were processed with the TIA (ThermoFisher), the DigitalMicrograph, and the JEMS (by P. Stadelmann) softwares. An Empyrean diffractometer (PanAnalytical) with Co K $\alpha_{1,2}$ was used for X-ray powder diffraction study. Electron energy-loss spectra were taken with a Gatan GIF with resolution of 0.9 eV. The X-ray photoelectron spectroscopy (XPS) (Kratos AXIS Supra) was carried out with a monochromatic Al K α (1486.7 eV) excitation source to determine the chemical composition and bonding environment of the sample. The CrystalMaker software was used for crystal structure and nanoparticle shape simulations (drawing, plots).

3. RESULTS AND DISCUSSION

3.1. XRD

The synthesized sample was analyzed using X-ray diffraction (**Figure 2**) confirming only the CeO₂ phase. The sample contained two morphological components. The first one contained \approx 5 nm CeO₂ nanoparticles (approximately 87 %, blue), the second one contained \approx 150 nm crystallites (green).

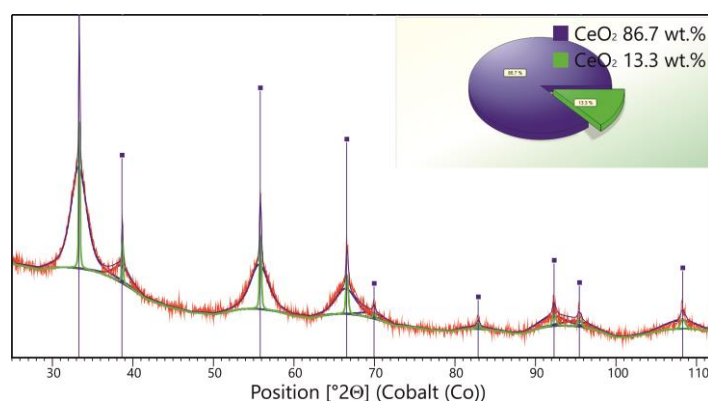


Figure 2 XRD patterns confirmed the CeO₂ phase and a high content of the nanocrystalline component (blue)

3.2. TEM

We purified the finest morphological component with centrifugal size fractionation to prepare TEM samples. We received approximately 100 nm nanoparticle clusters revealing individual nanoparticles at the cluster edges. TEM analysis revealed approximately 5 nm nanoparticles. We took 200 micrographs of 84 unduplicated nanoparticles at suitable orientations for facet type evaluation. The phase analyses using a Fast Fourier

transform pattern evaluation confirmed the CeO_2 phase. We observed octahedron shapes (**Figure 3a**) in most cases (approximately 80 %). All of these octahedrons were truncated, so $\{1,0,0\}$ facet types were observed in all nanoparticles. Truncated cuboctahedrons typically contained additional $\{1,1,0\}$ facets (**Figure 3b**). Some amounts of irregular nanoparticles were also observed (**Figure 3c**).

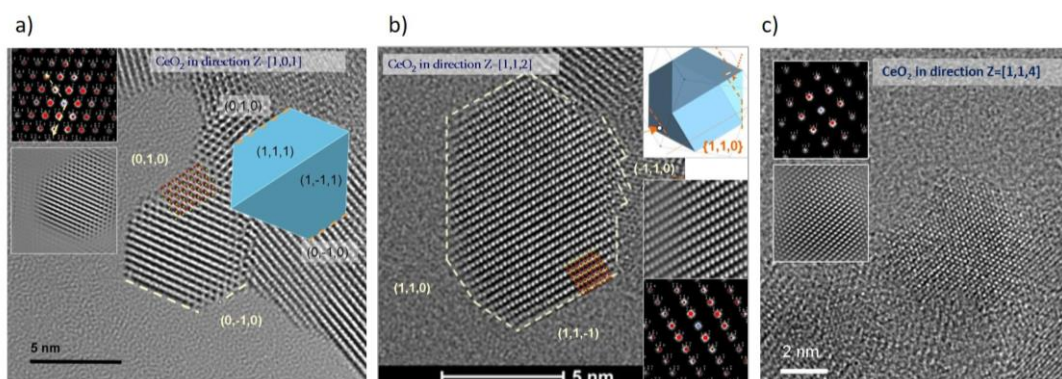


Figure 3 a) HRTEM image shows 5 nm truncated octahedron CeO_2 nanoparticle in crystallographic direction $Z = [1,0,1]$; b) truncated cuboctahedron in the direction $Z = [1,1,2]$ containing additional $\{1,1,0\}$ facet types, and c) irregular nanoparticle in the direction $Z = [1,1,4]$. Evaluated Fast Fourier transform patterns and Inverse filtered Fast Fourier patterns are included in the corresponding images

3.3. XPS

The XPS measurement proved the sample purity. Only the Ce and O were detected (**Figure 4a**). The visible peaks at the binding energies of 882.19 eV and 916.54 eV corresponded to $\text{Ce}^{4+} 3d_{5/2}$ and the 2nd satellite of $\text{Ce}^{4+} d_{3/2}$, respectively (**Figure 4b**). These energies indicated the CeO_2 phase content [9,10]. The identification of the $\text{Ce}^{3+} 3d_{5/2}$ and $\text{Ce}^{3+} d_{3/2}$ peaks was unclear. However, satellites at the energies of 884.26 eV and 902.69 eV confirmed the presence of Ce^{3+} . The O 1s spectra in more detail are visible in **Figure 4c**. These results suggested Ce^{4+} in majority compare to the Ce^{3+} compounds.

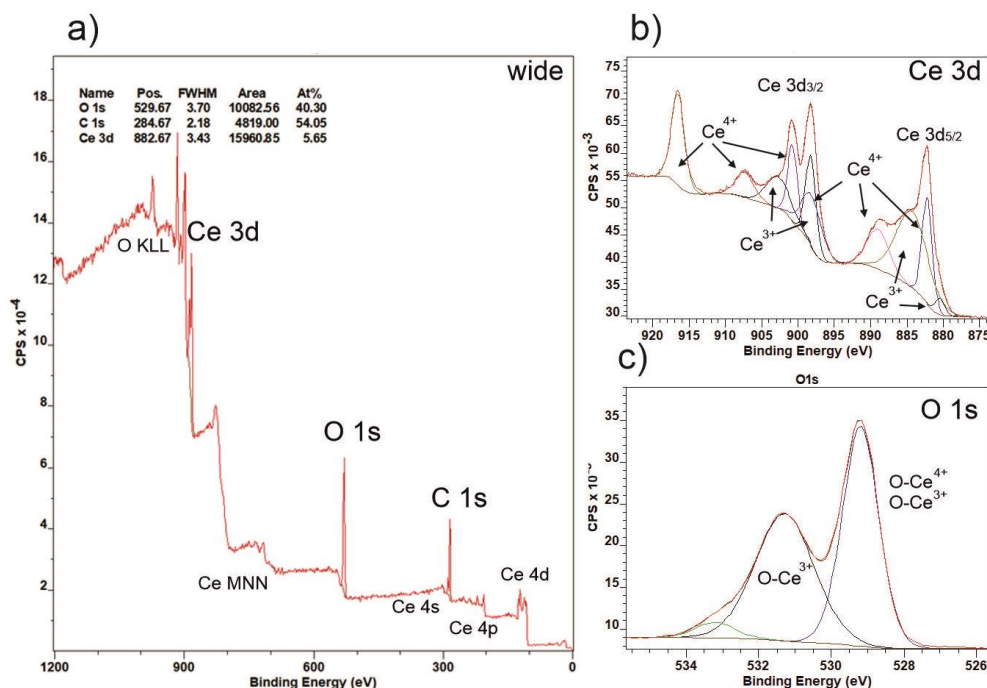


Figure 4 a) XPS wide spectra; b) Ce 3d; c) O1s spectra

3.4. EELS

EELS measurements were conducted in STEM mode and at an energy resolution of 0.9 eV. Data were taken from the thin areas of nanoparticle clusters near the surface. According to data received previously [11], we detected both oxidation states (**Figure 5**). The Ce^{3+} oxidation state was found as often as Ce^{4+} in the randomly chosen sites for analysis. These results indicate approximately equal representation of both states, contrary to XPS measurement results. This difference is intelligible because XPS measurements were conducted on the full sample surfaces, including large particles, in contrast to EELS data taken from the smallest nanoparticles at the cluster edge.

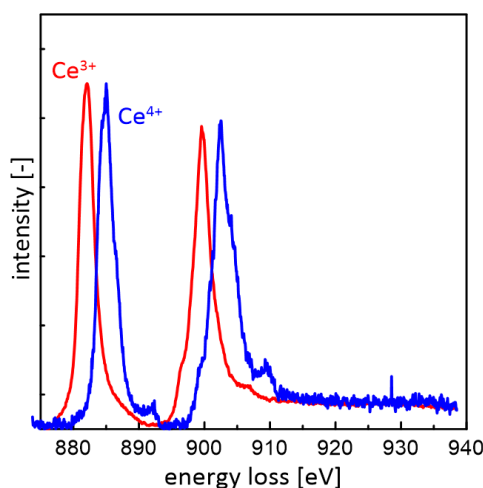


Figure 5 EELS measurements detect two oxidation states of cerium (Ce^{3+} and Ce^{4+})

4. CONCLUSION

This work confirmed the possible long-period redox activity of the samples prepared using electron beam evaporation. The results proved that nanoparticles formed with truncated shapes can be active in the redox processes for a long time. Nanoparticles maintained their morphology even after thermal treatment in the purification process. The phase analyses of many nanoparticles using FFT pattern evaluation confirmed only the CeO_2 phase. Therefore, the Ce^{3+} state is assumed to be in the nanoparticle surface layer formed with the off-stoichiometry CeO_{2-x} phase. The sample aging did not cause CeO_2 - Ce_2O_3 phase transformation even in the ultra-small nanoparticles.

ACKNOWLEDGEMENTS

The research has been supported by the Czech Science Foundation (Project 21-31852J) and by Russian Foundation for Basic Research (Project 20-58-26002). We acknowledge CzechNanoLab Research Infrastructure supported by MEYS CR (LM2018110).

REFERENCES

- [1] DHALL, A., SELF, W. Cerium oxide nanoparticles: A Brief Review of Their Synthesis Methods and Biomedical Applications. *Antioxidants (Basel)*. 2018, vol. 7, no. 8, pp. 97.
- [2] ULITKO, M.V., NAUMOVA, A.S., SULTANOVA, T.R., VAZIROV, R.A., AGDANTSEVA, E., OLSHVANG, O. Yu., SOKOVNIN, S. Yu. Investigation of the effect of cerium dioxide nanoparticles on the radiosensitivity of various cell types. *AIP Conference Proceedings*. 2020, vol. 2313, 080031.
- [3] XU, C., QU, X. Cerium oxide nanoparticle: a remarkably versatile rare earth nanomaterial for biological applications. *NPG Asia Mater*. 2014, vol. 6, no. e90.

- [4] SAIFI, M.A., SEAL, S., GODUGU, Ch. Nanoceria, the versatile nanoparticles: Promising biomedical applications. *Journal of Controlled Release*. 2021, vol. 338, pp.164-189.
- [5] DESHPANDE, S., PATIL, S., KUCHIBHATLA, S. VNT, SEAL, S. Size dependency variation in lattice parameter and valency states in nanocrystalline cerium oxide. *Appl. Phys. Lett.* 2005, vol. 87, 133113.
- [6] PÉREZ-BAILAC, P., LUSTEMBERG, P.G., GANDUGLIA-PIROVANO, M.V., Facet - dependent stability of near-surface oxygen vacancies and excess charge localization at CeO₂ surfaces. *Journal of Physics: Condensed Matter*. 2021, vol. 33, no. 50, 504003.
- [7] DAN, X., WANG Chao, XU Xi, LIU Ya, CHENG Xiaowei, FRONZI, M., BI Lei, ZHAO, X. S. Improving the sinterability of CeO₂ by using plane-selective nanocubes. *Journal of the European Ceramic Society*. 2019, vol. 39, pp. 4429-4434.
- [8] IL'VEZ, V.G., SOKOVNIN, S.Yu.. Production and studies of properties of nanopowders on the basis of CeO₂. 2012. *Nanotechnol. Russ.* 2012, vol. 7, pp. 213 - 226.
- [9] ELOIRDI, R., CAKIR, P., HUBER, F., SEIBERT, A., KONINGS, R., GOUDER, T. X-ray photoelectron spectroscopy study of the reduction and oxidation of uranium and cerium single oxide compared to (U-Ce) mixed oxide films. *Applied Surface Science*. 2018, vol. 457, pp. 566-571.
- [10] MASLAKOV, K.I., TETERIN, Yu.A., POPEL, A.J., TETERIN, A.Yu., IVANOV, K.E., KALMYKOV, N., PETROV, V.G., PETROV, V.G., PETROV, P.K., FARNAN, I. XPS study of ion irradiated and unirradiated CeO₂ bulk and thin film samples. *Applied Surface Science*. 2018, vol. 448, pp. 154-162.
- [11] GARVIE, L.A.J., BUSECK, P.R. Determination of Ce⁴⁺/Ce³⁺ in electron beam damaged CeO₂ by electron energy-loss spectroscopy. *Journal of Physics and Chemistry of Solids*. 1999, vol. 60, pp. 1943-1947.